Motion of a Spacecraft with Magnetic Damper

Carlos M. Roithmayr*
NASA Johnson Space Center, Houston, Texas 77058
Anren Hu†
Dynacs Engineering Company, Palm Harbor, Florida 34684
and
Richard Chipman‡
Grumman Corporation, Reston, Virginia 22090

Introduction

AN Earth-pointing spacecraft that is not at rest in a local-vertical–local-horizontal reference frame can, after a time, be brought nearly to rest by means of a device known as a magnetic damper consisting of a sphere, in which a permanent magnet is fixed, placed inside a spherical cavity attached to the spacecraft. The radius of the cavity is slightly larger than the radius of the sphere and the space in between is filled with a viscous fluid, typically silicone oil.

In what follows, three methods of numerically simulating motions of a spacecraft with a magnetic damper are compared; results obtained with the first approach are in general agreement with those based on the second approach, whereas results from the third method are incorrect unless the spacecraft is nearly at rest in a local-vertical–local-horizontal reference frame. We present a function that can be used (in the way an integral of equations of motion is sometimes used) to test the results of numerical integrations performed in connection with the first approach.

First Approach

The first approach, taken in Refs. 1 and 2, involves integrating a set of exact, coupled, nonlinear dynamical and kinematical differential equations of motion governing the behavior of the system S of two bodies shown in Fig. 1: a spacecraft C and a damper sphere D, in which a magnet of net dipole moment $\boldsymbol{m}$ is fixed. D^*, the mass center of D, is fixed in C and coincident with C^*, the mass center of C. Body C moves in Newtonian reference frame N.

We assume that C^* travels in a circular orbit around E^*, the mass center of E, the Earth, regarded as a particle for the purpose of computing gravitational force. In that event, Eqs. (6.1.2) of Ref. 3 lead to six dynamical equations of motion for S in N, three of which are satisfied by a single vector equation

$$\boldsymbol{I}\cdot{}^N\boldsymbol{\alpha}^C+{}^N\boldsymbol{\omega}^C\times\boldsymbol{I}\cdot{}^N\boldsymbol{\omega}^C-3\Omega^2\hat{\boldsymbol{a}}_1\times\boldsymbol{I}\cdot\hat{\boldsymbol{a}}_1-K^C\boldsymbol{\omega}^D=\boldsymbol{0}\qquad(1)$$

where $\boldsymbol{I}$ is the central inertia dyadic of C and ${}^N\boldsymbol{\alpha}^C$ and ${}^N\boldsymbol{\omega}^C$ denote, respectively, the angular acceleration and angular velocity of C in N. The term $3\Omega^2\hat{\boldsymbol{a}}_1\times\boldsymbol{I}\cdot\hat{\boldsymbol{a}}_1$ is an expression for the moment about C^* of the gravitational forces exerted by E on C, where $\hat{\boldsymbol{a}}_1$ is a unit vector in the direction of the position vector from E^* to C^* and Ω is a constant angular speed in N of a reference frame A in which $\hat{\boldsymbol{a}}_1$ is fixed. The set of contact forces exerted on C by the viscous fluid can be replaced by a couple whose torque is equal to $K^C\boldsymbol{\omega}^D$, where ${}^C\boldsymbol{\omega}^D$ is the angular velocity of D in C and K is referred to as a damping coefficient.

Received Nov. 6, 1993; revision received March 1, 1996; accepted for publication April 8, 1996.

*Aerospace Engineer, Vehicle Dynamics Section. Senior Member AIAA.
†Project Engineer; currently Staff Engineer, Welch Engineering Co., Rockville, MD 20850. Member AIAA.
‡Manager, Integrated Performance Analysis Branch, Space Station Division; currently Program Manager, Science Applications International Corp., McLean, VA 22102. Member AIAA.

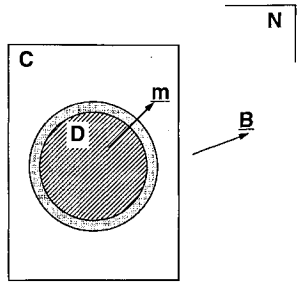

Fig. 1 Spacecraft and magnetic damper.

The remaining three dynamical equations governing motions of S in N are all satisfied by the vector equation

$$\boldsymbol{J}\cdot{}^N\boldsymbol{\alpha}^D-\boldsymbol{m}\times\boldsymbol{B}+K^C\boldsymbol{\omega}^D=\boldsymbol{0}\qquad(2)$$

where $\boldsymbol{J}$ is the central inertia dyadic of uniform sphere D and ${}^N\boldsymbol{\alpha}^D$ is the angular acceleration of D in N. The set of magnetic distance forces exerted on D can be replaced with a couple whose torque is $\boldsymbol{m}\times\boldsymbol{B}$, where $\boldsymbol{m}$ is the net dipole moment of the magnet fixed in D and $\boldsymbol{B}$ is the local magnetic field vector. The gravitational moment acting on D vanishes because D is regarded as a sphere whose mass is distributed uniformly.

The behavior of S in N is governed by several kinematical equations of motion, in addition to the six dynamical equations to which we have just alluded. Solutions of kinematical equations provide time histories of the orientations of C and D in A, which can be described with whatever variables the analyst finds convenient: orientation angles, direction cosines, Euler parameters (quaternions), or others.

The analyses undertaken with this approach in Ref. 4 make use of a variable step-size numerical integration algorithm designed specifically for systems of stiff ordinary differential equations; simulation results reported here have been obtained with the variable-coefficient ordinary differential equation solver.[5]

Checking Function

One may gain confidence in the results of numerical integrations of equations of motion by evaluating a checking function and verifying that it remains constant at every step of a solution. An affirmative result, although it does not guarantee validity, indicates that the equations of motion have been derived, encoded, and solved correctly. In some cases mechanical energy, angular momentum, or a Hamiltonian can serve as a checking function, but not in the present case. References 6 and 7 describe a way to obtain a scalar checking function C for any mechanical system. The validity of solutions of Eqs. (1) and (2) are checked with the function

$$C=\tfrac{1}{2}{}^N\boldsymbol{\omega}^C\cdot\boldsymbol{I}\cdot{}^N\boldsymbol{\omega}^C-{}^N\boldsymbol{\omega}^A\cdot\boldsymbol{I}\cdot{}^N\boldsymbol{\omega}^C+\tfrac{3}{2}\Omega^2\hat{\boldsymbol{a}}_1\cdot\boldsymbol{I}\cdot\hat{\boldsymbol{a}}_1$$
$$+\tfrac{1}{2}\Omega^2(I_3-3I_1)+\tfrac{1}{2}{}^N\boldsymbol{\omega}^D\cdot\boldsymbol{J}\cdot{}^N\boldsymbol{\omega}^D+Z\qquad(3)$$

where the angular velocity of A in N is given by ${}^N\boldsymbol{\omega}^A=\Omega\hat{\boldsymbol{a}}_3$; unit vector $\hat{\boldsymbol{a}}_3$ is perpendicular to $\hat{\boldsymbol{a}}_1$ and fixed in both A and N. The first four terms appearing on the right-hand side of the preceding equation are equivalent to the rotational Hamiltonian given in Eq. (3.5.21) of Ref. 8: it is an integral of the equations of motion of a rigid body whose mass center travels in a circular orbit, subjected solely to gravitational forces exerted by E. I_3 and I_1 denote, respectively, the largest and smallest central principal moments of inertia of body C. The final two terms appearing on the last line represent the contribution of the magnetic damper to the function C. Z is governed by a first-order differential equation,

$$\dot{Z}=K^C\boldsymbol{\omega}^D\cdot({}^N\boldsymbol{\omega}^D-{}^A\boldsymbol{\omega}^C)-{}^N\boldsymbol{\omega}^D\cdot\boldsymbol{m}\times\boldsymbol{B}\qquad(4)$$

which must be integrated simultaneously with all other equations of motion.

Second Approach

A second approach is based on the assumption that the resultant moment about D^* is zero and, therefore, that ${}^N\boldsymbol{\alpha}^D$ also vanishes. (The idea for this approach is not ours. Credit belongs to the Astro

Space Division of General Electric, Valley Forge, Pennsylvania. Unfortunately, we have been unable to obtain an appropriate reference to cite in this instance.) This assumption is used as a justification to jettison dynamical equations of motion associated with D, namely, the three obtained from Eq. (2); it leads to a relationship

$$^{C}\boldsymbol{\omega}^{D} = (\boldsymbol{m} \times \boldsymbol{B})/K \tag{5}$$

used at each integration step to recompute $^{C}\boldsymbol{\omega}^{D}$, which is then employed in kinematical equations for variables describing the orientation of D in C. Moreover, Eq. (1) gives way to

$$\boldsymbol{I} \cdot {}^{N}\boldsymbol{\alpha}^{C} + {}^{N}\boldsymbol{\omega}^{C} \times \boldsymbol{I} \cdot {}^{N}\boldsymbol{\omega}^{C} - 3\Omega^2 \hat{\boldsymbol{a}}_1 \times \boldsymbol{I} \cdot \hat{\boldsymbol{a}}_1 - \boldsymbol{m} \times \boldsymbol{B} = \boldsymbol{0} \tag{6}$$

after substituting from Eq. (5).

Third Approach

In the third approach, set forth in Refs. 9 and 10, D is presumed to move such that $\boldsymbol{m}$ is always parallel to $\boldsymbol{B}$; hence, dynamic and kinematic equations associated with D are left out of the picture entirely. This approach is based on the approximation

$$^{C}\boldsymbol{\omega}^{D} \approx \hat{\boldsymbol{b}} \times \frac{^{C}\mathrm{d}}{\mathrm{d}t}\hat{\boldsymbol{b}} \tag{7}$$

where $\hat{\boldsymbol{b}}$ is a unit vector in the direction of $\boldsymbol{B}$ and $^{C}\mathrm{d}\hat{\boldsymbol{b}}/\mathrm{d}t$ represents the derivative in reference frame C of $\hat{\boldsymbol{b}}$ with respect to time. Equation (7) appears as Eq. (22) of Ref. 9; from there, it can be traced to Eq. (18-64) of Ref. 10, and then to Eq. (9) of Ref. 11.

The third method replaces Eq. (6) of the second approach with

$$\boldsymbol{I} \cdot {}^{N}\boldsymbol{\alpha}^{C} + {}^{N}\boldsymbol{\omega}^{C} \times \boldsymbol{I} \cdot {}^{N}\boldsymbol{\omega}^{C} - 3\Omega^2 \hat{\boldsymbol{a}}_1 \times \boldsymbol{I} \cdot \hat{\boldsymbol{a}}_1 - K\hat{\boldsymbol{b}} \times \frac{^{C}\mathrm{d}}{\mathrm{d}t}\hat{\boldsymbol{b}} = \boldsymbol{0} \tag{8}$$

In Ref. 9, motions of C are partitioned into two categories: a despin or transient phase and a stabilized or steady-state phase. Equation (7) is shown to follow from Eq. (5) [also numbered Eq. (5) in Ref. 9] after the motion of C has been stabilized. Only then is it likely that $\boldsymbol{m}$ will remain nearly parallel to $\boldsymbol{B}$.

The third method is the basis for results of simulations of the motion of Space Station Freedom contained in Refs. 11 and 12; it is claimed in Sec. VII of Ref. 11, without substantiation of any sort, that the third approach produces results comparable to those from the first method. Absent from these two articles is a clear description of the circumstances, if any, under which $\boldsymbol{m}$ and $\boldsymbol{B}$ remain parallel. Furthermore, since the third method fails to provide any information whatsoever about the orientation of D, one never knows to what extent the direction of $\boldsymbol{m}$ differs from that of $\boldsymbol{B}$.

We show presently that Eq. (7) leads to reasonable results only when C is nearly at rest in local-vertical–local-horizontal reference frame A, and to incorrect results when C tumbles in A. Spacecraft such as the Long Duration Exposure Facility and Space Station Freedom must contend with plumes from a Space Shuttle's reaction control jets, which might induce tumbling.

Illustrative Examples

We now examine results from simulations based on each of the three approaches just described, to investigate their relative merits.

Let $\hat{\boldsymbol{p}}_1, \hat{\boldsymbol{p}}_2$, and $\hat{\boldsymbol{p}}_3$ be three dextral, orthogonal unit vectors fixed in C, parallel to central principal axes of inertia of C. Central principal moments of inertia of C are $I_1 = 60, 511$, $I_2 = 314, 126$, and $I_3 = 326, 518$ kg-m^2, where $I_r \triangleq \hat{\boldsymbol{p}}_r \cdot \boldsymbol{I} \cdot \hat{\boldsymbol{p}}_r (r = 1, 2, 3)$.

The central principal moment of inertia of D, used in connection with the first approach, is $J = 0.146$ kg-m^2. The magnitude of $\boldsymbol{m}$ is 1,125 A-m^2, while the value of K is 6.78 N-m-s.

If magnetic dampers are absent, C can remain at rest in A when, as is discussed in Sec. 3.5 of Ref. 8, $\hat{\boldsymbol{p}}_1$ is parallel to $\hat{\boldsymbol{a}}_1$ (local vertical), and $\hat{\boldsymbol{p}}_3$ is parallel to $\hat{\boldsymbol{a}}_3$ (normal to the orbit plane). Each simulation begins with this orientation of C in A. The orbit of C^* has a radius of 6783 km, which corresponds to an angular speed of $\Omega = 0.0646$ deg/s. The angle between the orbit plane and Earth's equatorial plane (inclination angle) is 28.5 deg. The initial latitude of C^* is 0 deg, and the initial longitude is −68.4 deg.

Simulations based on the first two approaches begin with $\boldsymbol{m}$ in the same direction as $\boldsymbol{B}$, and $^{C}\boldsymbol{\omega}^{D} = \boldsymbol{0}$. In the case of the third method, $^{C}\mathrm{d}\hat{\boldsymbol{b}}/\mathrm{d}t$ is initially $\boldsymbol{0}$.

The results that follow are obtained with a geocentric dipole model of the geomagnetic field [Eq. (H-22) of Ref. 10], and numerical values of the Gauss coefficients given in Ref. 13.

The absolute value of the checking function, which begins at zero, remains smaller than 2.3×10^{-11} N-m throughout the integrations performed for the first approach.

Spacecraft Nearly at Rest in Frame A

Simulation results from all three approaches are in agreement with one another when C is nearly at rest in frame A. An example of this kind of behavior can be produced by using the initial values $^{A}\boldsymbol{\omega}^{C} \cdot \hat{\boldsymbol{p}}_1 = -0.01$ deg/s, $^{A}\boldsymbol{\omega}^{C} \cdot \hat{\boldsymbol{p}}_2 = 0.01$ deg/s, and $^{A}\boldsymbol{\omega}^{C} \cdot \hat{\boldsymbol{p}}_3 = -0.01$ deg/s. Figure 2 shows a time history of θ, the angle between $\hat{\boldsymbol{p}}_1$ and $\hat{\boldsymbol{a}}_1$. Figure 3 depicts oscillations in β, the angle between $\boldsymbol{m}$ and $\boldsymbol{B}$, with an average value of 10 deg. Curves representing results from the second and third methods are absent from Fig. 2 because they are indistinguishable from the solid curve. Likewise, Fig. 3 does not contain a separate curve for the second method.

Although the phrase "nearly at rest" gives some qualitative indication of the circumstances under which the third method gives a valid solution, a precise discriminant is not readily available.

Vigorous Motion of Spacecraft

In this section we provide an example in which results obtained with the first and second approaches are in conflict with those from the third. Initial values $^{A}\boldsymbol{\omega}^{C} \cdot \hat{\boldsymbol{p}}_1 = -0.10$ deg/s, $^{A}\boldsymbol{\omega}^{C} \cdot \hat{\boldsymbol{p}}_2 = 0.10$ deg/s, and $^{A}\boldsymbol{\omega}^{C} \cdot \hat{\boldsymbol{p}}_3 = -0.10$ deg/s lead to motions in which C pirouettes and tumbles in A. C is said to tumble when θ grows larger than 90 deg. The first and second approaches lead to the curves for θ shown in Fig. 4 where tumbling of C is in evidence almost immediately and continues for approximately six orbits. C performs a number of complete somersaults, after which θ approaches 0 deg, rather than 180 deg. Figure 5 shows that β reaches 55 deg during the first orbit, a signal that there will be trouble with the third approach.

Figure 6 reveals a marked difference between time histories of θ obtained by using the first and third techniques. The discrepancy is apparent shortly after the second orbit. The first approach indicates

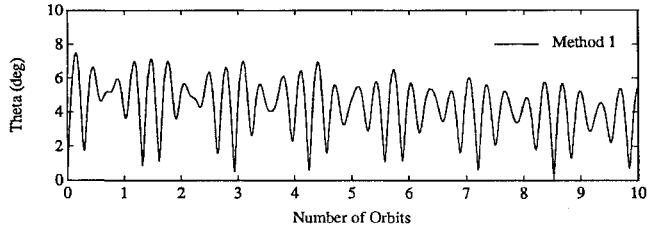

Fig. 2 Spacecraft nearly at rest.

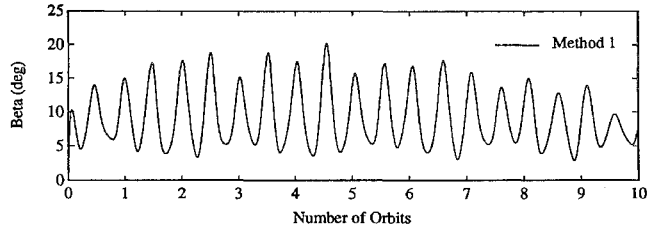

Fig. 3 Angle between dipole and field.

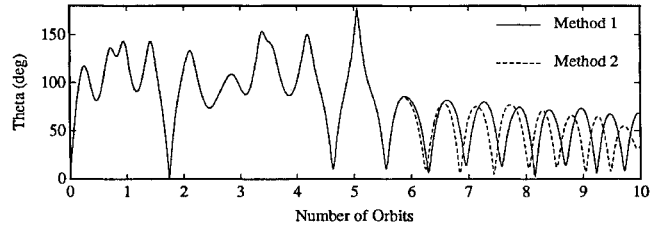

Fig. 4 Vigorous motion, methods 1 and 2.

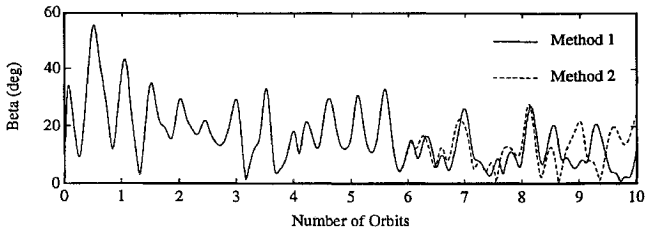

Fig. 5 Angle between dipole and field.

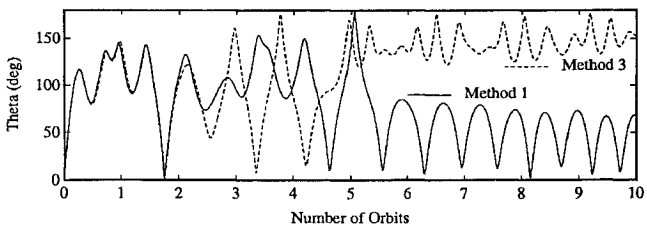

Fig. 6 Vigorous motion, methods 1 and 3.

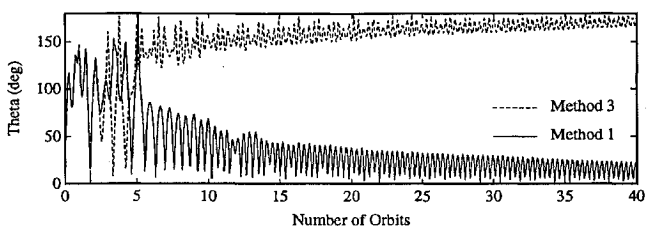

Fig. 7 Methods 1 and 3, 40 orbits.

C is right side up during orbits 6–10 because θ is less than 90 deg, whereas the third approach leads to the erroneous conclusion that C is upside down during that time.

The simulation mentioned in Refs. 11 and 12 employed fixed step numerical integration; steps of 0.2, 0.1, 0.05, and 0.02 s all produce the broken curve in Fig. 6, but they lead to different solutions after the 12th orbit.

The problem of numerical stability notwithstanding, another defect in the third method comes to light upon examining results beyond the 15th orbit. In view of Fig. 7, the first technique predicts excursions of θ to be approximately 20 deg in the neighborhood of orbit 40. The second method, whose results are not illustrated here, yields basically the same prognosis. In contrast, the broken curve shows that the third method, together with a step size of 0.02 s, leads to the mistaken conclusion that the excursions of θ are less than 15 deg at that time.

An earlier version of this Note[14] inadvertently displayed results for the third method that, in the case of vigorous motion, were obtained with $K = 1.36$ N-m-s. Only the broken curves in Figs. 6 and 7 contained the mistake, and they are now correct.

Conclusions

Two methods of modeling the action of a magnetic damper on a spacecraft, which take into account the motion of the damper sphere, produce simulation results that are in general agreement. A checking function for equations governing the motion of a spacecraft and damper sphere is used to bolster confidence in results of numerical integrations required by the first technique. A third method, in which the motion of the damper sphere is completely ignored, furnishes unacceptable results unless the spacecraft is nearly at rest in a local-vertical–local-horizontal reference frame. Solutions obtained with the third approach are shown to contain significant errors when the spacecraft tumbles. In the absence of a precise quantitative criterion that indicates whether a particular simulation will produce valid results, it seems best to dispense with the third approach altogether.

References

[1]Breedlove, W. J., and Heinbockel, J. H., "A Formulation of the Equations of Motion for the Long Duration Exposure Facility (LDEF)," TR 74-M3, Old Dominion Univ., Norfolk, VA, July 1974.

[2]Das, A., Foulke, H. F., and Siegel, S. H., "Passive Stabilization of the Long Duration Exposure Facility (LDEF)," General Electric Co., GE 74SD4264, Valley Forge, PA, Nov. 1974.

[3]Kane, T. R., and Levinson, D. A., *Dynamics: Theory and Applications*, McGraw–Hill, New York, 1985.

[4]Heinbockel, J. H., and Breedlove, W. J., "An Analysis of the Passive Stabilization of the Long Duration Exposure Facility (LDEF)," School of Engineering, TR 74-M5, Old Dominion Univ., Norfolk, VA, Sept. 1974.

[5]Brown, P. N., Byrne, G. D., and Hindmarsh, A. C., "VODE, A Variable-Coefficient ODE Solver," *SIAM Journal on Scientific and Statistical Computing*, Vol. 10, No. 5, 1989, pp. 1038–1051.

[6]Kane, T. R., and Levinson, D. A., "A Method for Testing Numerical Integrations of Equations of Motion," *Journal of Applied Mechanics*, Vol. 55, No. 3, 1988, pp. 711–715.

[7]Kane, T. R., and Levinson, D. A., "Testing Numerical Integrations of Equations of Motion," *Journal of Applied Mechanics*, Vol. 57, No. 1, 1990, pp. 248, 249.

[8]Kane, T. R., Likins, P. W., and Levinson, D. A., *Spacecraft Dynamics*, McGraw–Hill, New York, 1983.

[9]Pettus, W. W., "Performance Analyses of Two Eddy Current Damping Systems for Gravity-Gradient Stabilized Satellites," *Proceedings of the Symposium on Gravity-Gradient Attitude Stabilization*, The Aerospace Corp., El Segundo, CA, 1968, pp. 3-67–3-82.

[10]Wertz, J. R. (ed.), *Spacecraft Attitude Determination and Control*, D. Reidel, Dordrecht, The Netherlands, 1978.

[11]Wade, J. W., "Passive Attitude Damping of Alternative Assembly Configurations of Space Station Freedom," *Journal of Guidance, Control, and Dynamics*, Vol. 14, No. 1, 1991, pp. 36–43.

[12]Wade, J. W., "Attitude Oscillation Damping for Space Station Freedom Alternative Assembly Configurations," *Proceedings of the Eighth American Control Conference*, Vol. 2, Inst. of Electrical and Electronics Engineers, New York, 1989, pp. 1573–1578.

[13]Anon., *Space Station Program Natural Environment Definition for Design*, SSP 30425 Rev. A, NASA Space Station Freedom Program Office, Reston, VA, June 1991, p. 9-6.

[14]Roithmayr, C. M., Hu, A., and Chipman, R., "Motion of a Spacecraft with Magnetic Damper," *Proceedings of the AIAA/AAS Astrodynamics Conference*, AIAA, Washington, DC, 1992, pp. 38–46.